Influence of thermal stress relief parameters on crystallographic distortion and energy absorption behavior of closed-cell aluminium alloy foams

Dewi Puspitasari[1]*, *Mazli* Mustapha[2], *Turnad* Lenggo Ginta[3], and *Andita* Nataria Fitri Ganda[1]

[1]Applied Mechanical Engineering, Faculty of Vocational Studies, Universitas Negeri Surabaya, East Java, Indonesia
[2]Mechanical Engineering Department, Faculty of Engineering, Universiti Teknologi Petronas, Perak, Malaysia
[3]Research Center for Process and Manufacturing Industry Technology, National Research and Innovation Agency, Banten, Indonesia

Abstract. Aluminium foams offer lightweight structural advantages for energy absorption applications; however, residual stresses from foaming processes can degrade mechanical reliability and crystallographic integrity. This research addresses the problem by examining how thermal stress-relieving parameters affect the structural and energy-absorption performance of closed-cell aluminium alloy foams. The research contribution is the establishment of a clear correlation between lattice distortion, precipitate evolution, and compressive energy-absorption characteristics following low-temperature stress-relieving treatments. Three conditions were evaluated: as-received foam, stress relief at 500 °C for 60 min, and stress relief at 550 °C for 120 min. Mechanical behavior was examined through quasi-static compression tests, while crystallographic modifications were analyzed using X-ray diffraction and Williamson-Hall calculations. The 500 °C-60 min treatment improved compressive strength from 1.35 N/mm² to 2.88 N/mm² and enhanced energy absorption by 95%, attributed to refined and uniformly distributed precipitates that increased lattice integrity and reduced internal stresses. In contrast, excessive exposure at 550 °C for 120 min led to precipitate coarsening and a reduction in strength. XRD peak shifts confirmed changes in lattice strain resulting from thermal exposure. This study demonstrates that optimized thermal stress relief significantly improves mechanical reliability and provides insights for designing crash-resistant, load-bearing aluminium foam structures.

1 Introduction

Aluminium foams have received growing attention as multifunctional materials in engineering systems where weight savings, safety performance, and energy efficiency are critical design priorities [1]. Their ability to combine low density with superior energy absorption and thermal resistance makes them attractive in the aerospace and automotive sectors, especially in protective elements such as crash absorbers, stiffened panels, and lightweight load-bearing components. Unlike dense aluminium alloys, the mechanical characteristics of aluminium foams originate from a combination of cell geometry, solid-state deformation mechanisms, and crystallographic behavior at the cellular scale [2]. This interplay between architecture and crystallography makes aluminium foam a compelling platform for studying the physics of deformation in porous metals.

However, the fabrication of aluminium foam—whether through casting, powder metallurgy, or gas-based expansion—often introduces residual stresses, uneven solute distributions, and crystallographic defects due to rapid thermal gradients and gas entrapment [3], [4]. These internal stresses reduce the lattice spacing and weaken the foam's load-bearing capacity, leading to premature local collapse and decreased energy absorption during dynamic or compressive loading [5], [6]. For applications where crashworthiness or vibration resistance is critical, managing residual stress becomes an essential design factor.

Thermal treatments are widely applied to improve microstructural uniformity in aluminium-based systems. Methods such as solution heat treatment and artificial aging can increase strength through controlled precipitation hardening [7]. Yet, higher-temperature treatments risk over-aging, pore distortion, and undesirable phase evolution that may degrade the mechanical stability of the cell walls [8]. A more suitable alternative is thermal stress-relieving, which aims to relax residual stress at lower temperatures while preserving the pore architecture and supporting microstructural refinement [9], [10]. In aluminium foam, the highly heterogeneous pore network leads to a heat-induced microstructural response that differs from that of fully dense alloys, making a systematic investigation essential.

Previous studies have indicated that variations in pore wall thickness, precipitate distribution, and porosity affect hardness, compressive strength, and

* Corresponding author: dewipuspitasari@unesa.ac.id

plateau behavior [11]. Analytical techniques such as X-ray diffraction (XRD) and elemental mapping enable direct observation of lattice strain relaxation, changes in crystallite size, and solute redistribution during thermal exposure [12], [13], [14]. However, the combined influence of stress-relieving parameters on both crystallographic distortion and energy absorption capacity in closed-cell foams remains insufficiently investigated.

Therefore, this work examines how different thermal stress-relieving conditions affect hardness, compressive energy absorption, and lattice strain in closed-cell aluminium alloy foam. The primary contribution of this research is the quantitative correlation between crystallographic relaxation and improved deformation stability, offering scientific and practical insights into tailoring thermal post-processing for lightweight structures subjected to extreme mechanical demands.

2 Materials and methods

The experimental procedure for this study consisted of four main stages, as shown in Figure 1. The process began by preparing aluminium foam (Al-foam) to ensure controlled porosity and a uniform structure. Next, thermal stress relief was performed in a furnace to reduce residual stresses and improve material stability. The testing phase involved mechanical characterization, including hardness and compressive strength tests, to assess the foam's structural and mechanical behavior. Finally, data analysis was conducted to interpret the results, identify trends, and relate microstructural features to mechanical performance.

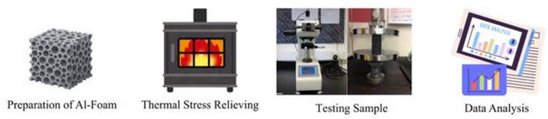

Fig. 1. Experimental procedure.

2.1 Material

The material used in this study was a commercially available closed-cell aluminium alloy foam (Alporas type), produced by the foaming-melting process with a chemical blowing agent. The fabrication process began with the melting of high-purity aluminium, followed by the addition of 1.5 wt% calcium (Ca) to increase the viscosity of the molten aluminium, thereby stabilizing the foam structure during expansion. Subsequently, 1.6 wt% titanium hydride (TiH_2) was added as a blowing agent. Upon thermal decomposition, TiH_2 released hydrogen gas, which expanded the molten metal and formed the foam, while leaving behind a solid titanium residue dispersed in the matrix.

2.2 Composition and element mapping of Aluminium Foam Measurement

The bulk chemical composition of the closed-cell aluminium alloy foam was determined using X-Ray Fluorescence (XRF). In contrast, the surface elemental composition of the foam cell wall was analyzed using the SEM's built-in Energy-Dispersive X-ray Spectroscopy (EDX).

2.3 Stress relieving heat treatment

In this study, a thermal stress-relieving procedure was conducted using a vacuum furnace. The objective of this treatment was to alleviate internal residual stresses in the aluminium foam while maintaining its cellular structure. The experimental parameters were selected based on a simplified design matrix comprising specific values for heating temperature, holding time, and stabilization temperature.

The process began by heating the specimens from ambient temperature (25 °C) to a predefined stabilization temperature of 350 °C or 450 °C at a constant heating rate of 10 °C/min. Once the stabilization temperature was reached, the samples were held for 20 minutes to ensure uniform thermal distribution throughout the foam. The temperature was then increased—again at a rate of 10 °C/min—until the target stress-relieving temperature (either 500 °C or 550 °C) was reached. This temperature was maintained for a designated holding period of either 60 or 120 minutes, depending on the treatment group. This process is illustrated in Figure 2. Finally, all samples were allowed to cool gradually inside the furnace (furnace cooling) to prevent thermal shock and distortion.

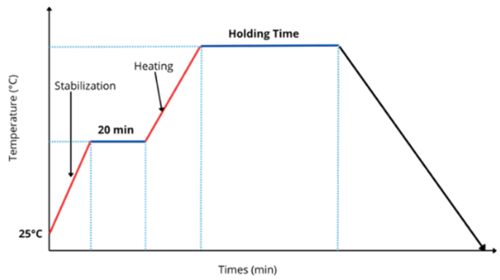

Fig. 2. Schematic diagram of stress relieving heat treatment.

All heat treatments were carried out under vacuum conditions at a fixed pressure of 114 mTorr, which helped prevent oxidation and ensured a clean thermal environment. The detailed parameter settings, including temperature and time segments, are presented in Table 1. This carefully controlled thermal cycle provided a consistent basis for investigating the influence of stress relieving on the microstructural and physical behavior of the aluminium foam, particularly in relation to hardness, compressive strength, crystallographic structure, and energy absorption capability.

Table 1. Parameters setting for stress relieving heat treatment.

Run No.	Heating Temperature (°C)	Holding Time (min)	Stabilization Temperature (°C)
1.	As received	As received	As received
2.	500	60	450
3.	550	120	350

2.4 Hardness measurement

Microhardness measurements were performed on the cell wall nodes of the aluminium foam in accordance with ASTM E92 using a LM24AT microhardness tester. A load of 150 mN was applied for 15 seconds. For each node, five indentations were made to ensure accuracy, and the average value was used for analysis. During the test, the load was applied gradually and released smoothly to prevent surface damage. After unloading, the two diagonals of the indentation were measured, and their average was used to calculate the Vickers hardness (HV) value based on Equation (1) [15].

$$HV = \frac{2000P\, sin\left(\frac{\alpha}{2}\right)}{d^2} = \frac{1.854\, P}{d^2} \quad (1)$$

2.5 Compressive mechanical properties determination

A quasi-static compression test was performed using a universal testing machine (UTM) with a maximum load capacity of 5 kN, integrated with a computer-based data acquisition and control system. All compression tests were conducted at a crosshead speed of 1 mm/s, in accordance with ASTM D1621-00, which outlines procedures for determining the compressive properties of rigid cellular plastics.

From the resulting stress–strain curves, key parameters, including compressive strength, plateau stress, and densification strain, were extracted. The nominal stress was calculated by dividing the applied load by the specimen's original cross-sectional area. In contrast, the nominal strain was obtained by dividing the displacement of the crosshead by the specimen's initial height [16].

The compressive strength (σ_γ) was defined as the maximum stress at the end of the elastic region, just before the onset of permanent deformation, or equivalently, the first distinct peak on the stress–strain curve [17].

The plateau stress (σ_{pl}) was calculated as the average stress between 5% and 30% strain, representing the region where the foam undergoes stable plastic collapse [14]. Additionally, the energy absorption capacity (W) of the foam was determined by calculating the area under the stress–strain curve up to the onset of densification, using Equation (2).

$$W = \int_0^{\varepsilon_d} \sigma(\varepsilon) d\varepsilon \quad (2)$$

The densification strain (ε_d) was calculated when all the cell walls have collapsed and flattened. It was taken at the intersection of the plastic deformation plateau and the densification loading [18].

2.6 Lattice strain and crystallite measurement

The lattice strain and crystallite size of the closed-cell aluminium alloy foam were quantified using a PANalytical X'Pert³ Powder X-ray Diffractometer (Cu Kα radiation, λ = 0.15406 nm), measuring diffraction angles (2θ) from 10° to 90°. Crystallographic phases were identified through HighScore Plus software, and measured d-spacing values were matched with standard patterns from the ICDD-PDF database. To determine crystallite size and lattice strain, the Williamson–Hall plot method was applied, which separates broadening of diffraction peaks into components arising from finite crystallite size and micro strain [19].

3 Results and discussion

This section presents the study's results in a structured manner, starting with the elemental composition of the closed-cell aluminium alloy foam, then its mechanical behavior, and finally its crystallographic characteristics.

3.1 Composition of aluminium foam

The chemical composition of the aluminium foam, analyzed by XRF (Figure 3), reveals aluminium (Al) as the dominant element at 65.4 wt%, establishing the alloy's base matrix. Calcium (Ca) at 18.7 wt% is present in significant amounts, added to increase the melt's viscosity during the foaming process, thereby improving pore stability. Iron (Fe), titanium (Ti), and zinc (Zn) are also observed at 6.6 wt%, 3.44 wt%, and 2.29 wt%, respectively, playing essential roles in modifying mechanical strength and contributing to the structural integrity of the foam. Minor elements such as silicon (Si), phosphorus (P), and magnesium (Mg) are present in trace amounts (<1 wt%) and may influence grain boundary behavior and corrosion resistance.

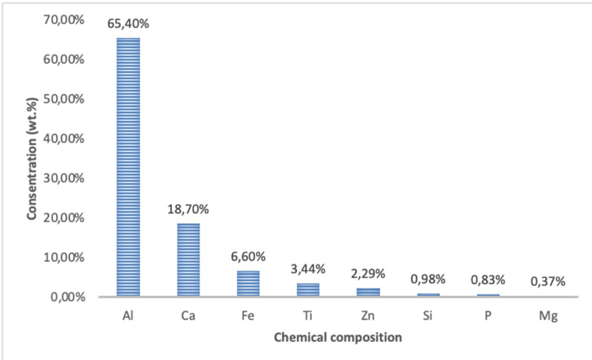

Fig. 3. Chemical composition of aluminium foam.

Complementing the bulk analysis, surface composition from EDS (Figure 4) indicates the presence of Al (52.7 wt%), Ca (6.6 wt%), Ti (1.0 wt%), oxygen (19.3 wt%), and carbon (18.0 wt%). The significant oxygen and carbon peaks likely originate from oxide layers or organic residues on the surface, possibly introduced during processing or exposure to ambient conditions. These surface oxides can impact bonding behavior and may affect foam stability or surface interactions in service.

Together, the XRF and EDS data confirm the alloy's composition aligns with the known formulation of Alporas-type foams, where metallic additives like Ca and Ti serve dual functions in foam stabilization and structural reinforcement, while trace elements fine-tune the foam's final mechanical performance.

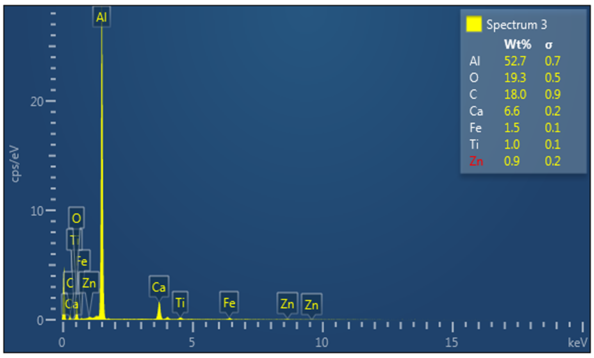

Fig. 4. Chemical composition of aluminium foam.

3.1.1. Element mapping run 1

The results are presented in Figure 5. From the SEM-EDX elemental images, it can be observed that traces of Ca, Fe, Ti, and Si exhibit a homogeneous distribution in the Al matrix. Al and Ca were detected from the dendritic and eutectic regions. Fe and Ti were scattered in the particle region, while Si was detected at the particle and eutectic regions. As shown in Table 2, the concentration of Carbon was dominant in the dark area, and it was believed to be epoxy resins. The oxygen analysis revealed that an oxide layer had formed in the as-received sample (Run 1). The distribution of elements within the cell wall of run 1 is illustrated in Figure 6.

Table 2. The concentration of elements in the run one aluminium alloy foam shown in figure**.**

Spectrum No	Concentration of Element (Weight %)					
	C	O	Al	Si	Ca	Ti
1	73.35	21.56	1.59	1.88	1.62	0
2	10.73	5.79	69.23	13.73	0.22	0.3
3	6.24	17.29	67.33	2.19	6.94	0

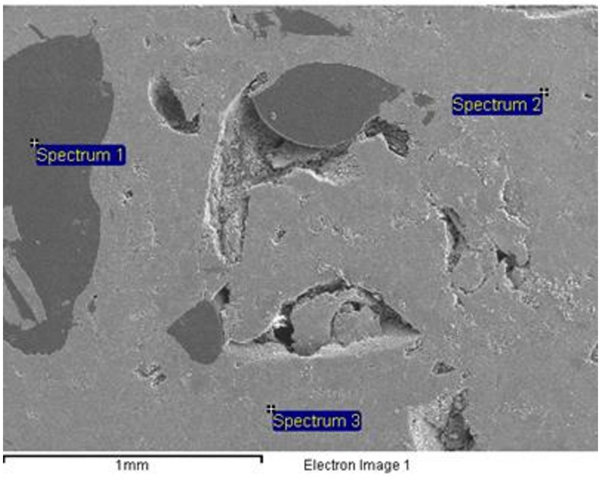

Fig. 5. Map of EDX spot analysis of the Run 1 aluminium alloy foam.

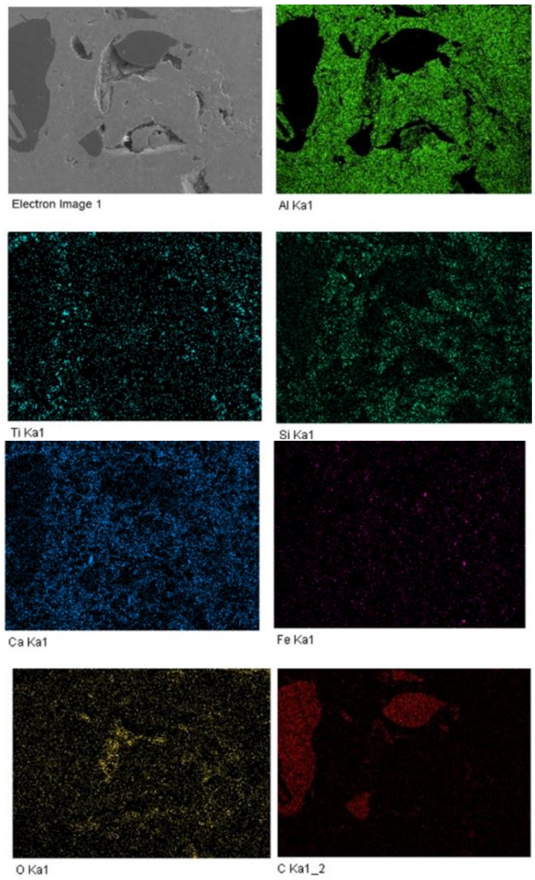

Fig. 6. EDX image of an area showing the distribution of elements within the cell wall of the run 1 sample.

3.1.2. Element mapping run 2

The EDX spots analysis was conducted on the dark and grey regions of the cell wall surface, as shown in Figure 7. The entire cell wall surface was analyzed at three random locations. The concentration of an element on each spectrum is summarized in Table 3. From the results, aluminium was the dominant element, and the maximum concentration of Si was observed in spectrum 2, while the maximum concentration of Ti was observed in spectrum 1.

Figure 8 shows energy dispersive X-ray (EDX) images of the Std 5 specimen. From the EDX images, traces of Ca, Fe, and Si were uniformly distributed in the Al matrix. The traces of titanium (Ti) formed clusters of micrometer size. The oxide layer also appeared in this sample, indicating the presence of the Al2O3 phase. The calcium region observed in the specimen was believed to have originated from CaO and Al2CaO4. The Al-Ca-Ti-Fe particle was also found in this sample.

Table 3. The concentration of elements in run 2 aluminium foam is shown in figure.

Spectrum No	Concentration of Element (Weight %)					
	O	Al	Si	Ca	Ti	Mg
1	2.15	50.04	0	3.69	44.11	0
2	1.09	56.5	42.41	0	0	0
3	14.38	65.92	0	18.59	0	1.11

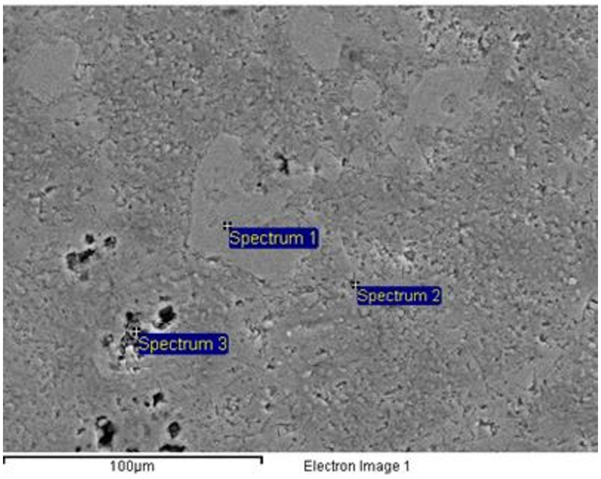

Fig. 7. Map of EDX spot analysis of the Run 2 aluminium foam.

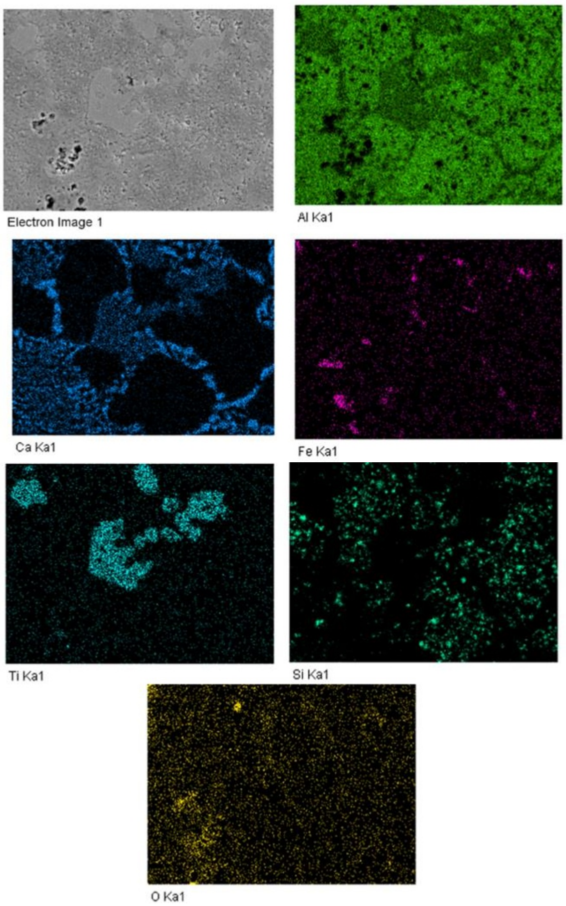

Fig. 8. EDX image of an area showing the distribution of element within the cell wall of run 2 sample.

3.1.3. Element mapping run 3

Figure 9 displays the SEM-EDX spot analysis image of the Run 3 aluminium foam. To determine the elemental composition within specific regions of the cell wall surface, EDX spot analysis was conducted. Three distinct locations—characterized by varying shades of grey—were randomly selected for this analysis. The elemental concentrations obtained from these spectra are summarized in Table 4. Across all measured points, aluminium was consistently the predominant element, as further illustrated in the elemental distribution shown in Figure 10. As anticipated, aluminium showed a high intensity in all spectra, while spectrum 2 also revealed a notable concentration of silicon (Si), indicating localized enrichment in that area.

An energy-dispersive X-ray (EDX) spectrum of the run sample is shown in Figure 8. EDX images were employed to investigate the chemical composition of the closed-cell aluminium alloy foam. For the Run 3 specimen, traces of calcium (Ca), titanium (Ti), and silicon (Si) were generally distributed in the aluminium matrix. The Si element was also detected and appeared as clusters of micrometer size. The Al2O3 oxide layer was also detected in this analysis spot. Iron (Fe) was not detected during the investigation.

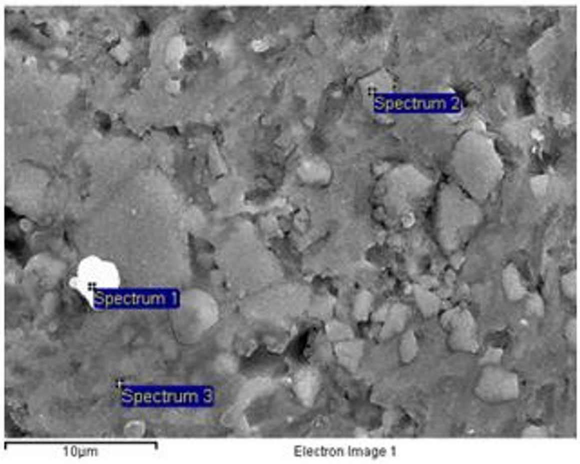

Fig. 9. Map of EDX spot analysis of the Run 3 aluminium foam.

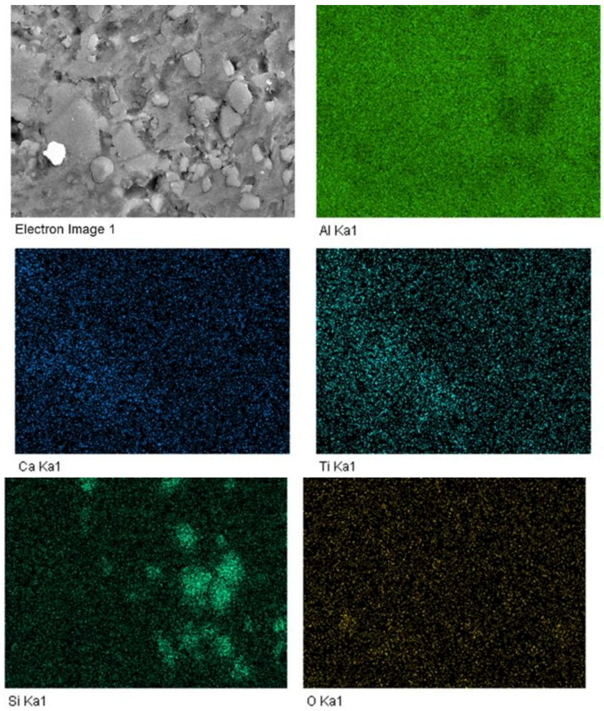

Fig. 10. EDX image of an area showing the distribution of elements within the cell wall of the run 3 sample.

Table 4. The concentration of elements in run 3 aluminium foam shown on figure.

Spectrum No	Concentration of Element (Weight %)				
	O	Al	Si	Ca	Ti
1	38.26	52.42	2.35	4.13	2.85
2	3.53	46.47	50	0	0
3	4.38	94.83	0	0.38	0.42

3.2 Hardness properties

The investigation into the hardness of aluminum specimens subjected to different stress-relieving treatments reveals significant findings that illustrate the role of thermal processing in microstructural evolution, particularly regarding precipitation mechanics, as tabulated in Table 5.

Table 5. Mechanical properties of aluminium foam.

Run No	Hardness	Compressive Strength	Plateau Stress	Energy
	HV	N/mm^2	N/mm^2	J
1	85.16	1.35	1.71	59.82
2	192.78	2.88	2.35	116.79
3	104.68	1.07	1.68	64.52

The specimen that underwent stress relieving at 550 °C for 60 minutes, followed by stabilization at 450 °C, showed the most remarkable hardness improvement. Hardness measurements indicated an increase of up to approximately 120% compared to as-received materials. This enhancement is attributed to the formation of fine, uniformly distributed precipitates within the aluminum matrix, thereby significantly increasing the volume fraction of these strengthening phases. The literature supports the claim that fine, needle-like β’’ precipitates contribute effectively to strengthening an aluminum matrix by improving load transfer and preventing dislocation movement, which is central to enhancing hardness [20]. Specifically, Rakhmonov et al. indicate that uniformly distributed fine precipitates with a diameter around 4 nm enhance the mechanical Performance of aluminum alloys through effective dispersoid strengthening [20].

On the other hand, the treatment that yielded the lowest hardness involved maintaining the same heating temperature of 550 °C, extending the holding time to 120 minutes, and lowering the stabilization temperature to 350 °C. This condition led to the formation of coarser precipitates, thereby diminishing hardness. The reduction in hardness is closely linked to the poor effectiveness of precipitation hardening, caused by increased spacing between precipitate particles that hinders the load-bearing capability of the matrix and dislocation interactions. This observation aligns with findings from Xu et al. (2020), who noted that prolonged heat treatment can enlarge precipitates, thereby reducing their strengthening effects [21]. Furthermore, Kim et al. support this by emphasizing that larger precipitate phases may not be as effective at enhancing strength due to reduced interparticle interaction surfaces, thereby weakening the overall microstructural integrity [22].

3.3 Compressive mechanical properties

The mechanical performance of aluminium foam under varying thermal conditions has shown significant implications for its compressive strength, plateau stress, and energy absorption capabilities, as shown in Table 2. In its as-received state, the aluminium foam exhibited baseline mechanical properties, including a compressive strength of 1.35 N/mm², a plateau stress of 1.71 N/mm², and an energy absorption capacity of 59.82 J. The original microstructure of the foam at this stage retains potential residual stresses and unoptimized cell morphologies, which influence its performance metrics [10].

Upon thermal treatment at 500 °C for 60 minutes, followed by stabilization at 450 °C, substantial improvements were observed. The compressive strength increased to 2.88 N/mm², plateau stress rose to 2.35 N/mm², and energy absorption capacity nearly doubled to 116.79 J. This enhancement can be attributed to the formation of a refined microstructure, likely due to evenly dispersed precipitates within the aluminium matrix, which promotes mechanical stability and energy dissipation during loading. The moderate heating and sufficient holding time seemingly allowed the internal structure of the foam to achieve greater homogeneity, enhancing its load bearing and energy-dissipating qualities, aligning with previous studies that emphasize the critical role of thermal treatment in optimizing the properties of aluminium foams [16].

In contrast, when the foam was treated at 550 °C for 120 minutes, followed by stabilization at 350 °C, the results were detrimental to its mechanical performance. The compressive strength decreased to 1.07 N/mm², lower than the initial as-received condition, while the plateau stress only slightly decreased to 1.68 N/mm², and energy absorption improved to 64.52 J. These results indicate that prolonged exposure to excessive temperatures led to precipitate coarsening and possible over-aging, ultimately compromising the foam’s structural integrity [23].

These findings underscore the need to optimize heat-treatment parameters for aluminium foams. Moderate heating temperatures combined with controlled holding times and stabilization phases can lead to significant improvements in mechanical performance. Conversely, aggressive thermal conditions, particularly over extended periods, can lead to structural inefficiencies and diminished energy-absorption capabilities. This body of work highlights the delicate balance required in the thermal processing of aluminium foam to maximize its mechanical properties, thereby enhancing its application potential in fields such as automotive and aerospace engineering [1], [24].

3.4 Lattice strain and crystallite properties

In the examination of aluminium alloy foam samples (Run 1, Run 2, and Run 3) using X-ray Diffraction (XRD), the results are presented in Figure 11. The observed phase composition revealed the presence of four primary phases: α-aluminium (α-Al), aluminium calcium (Al_4Ca), aluminium iron titanium

$(Al_{0.9}Fe_{3.1})Ti_2$, and silicon oxide (SiO_2). The results are presented in Table 6. The diffraction patterns indicated that the α-Al phase exhibited the highest-intensity peaks, suggesting its predominant presence in the alloy. The lower reflection intensities of Al_4Ca, $(Al_{0.9}Fe_{3.1})Ti_2$, and SiO_2 compared to α-Al reaffirm typical patterns found in XRD analyses, where the most stable phase often dominates the diffraction profile [25], [26].

Furthermore, the data illustrated a notable shift in the main α-Al peak toward lower intensity in the diffraction patterns from Run 2 and Run 3 compared to Run 1. This shift can be attributed to subtle variations in the aluminium lattice parameters, which may have resulted from induced lattice strain or distortion due to the stress-relieving heat treatment applied to the samples. Such alterations in lattice parameters have been documented in studies exploring structural changes caused by thermal treatments, in which heat exposure can significantly modify the crystalline architecture of aluminium foams and alloys. However, suitable references specifically addressing these changes in aluminium foams with heat treatment are not included in the provided references [26], [27].

The concept of thermal treatment altering the crystal structure is supported by the literature on the effects of heat on aluminium materials. Enhancements in mechanical properties and microstructural refinement through controlled heating processes are well documented [28]. The relationship between thermal exposure and the resulting modifications in the crystalline structure of aluminium has been reported in various studies; however, the specific connection to aluminium foam treatments requires further direct supporting evidence [29].

Table 6. The details of phases on closed-cell aluminium alloy foam.

Compound Name	Chemical Formula	Crystal System
Aluminum	Al	Cubic
Aluminum Calcium	Al4 Ca	Tetragonal
Aluminum Iron Titanium	(Al0.9 Fe3.1) Ti2	Hexagonal
Silicon Oxide	Si O2	Hexagonal

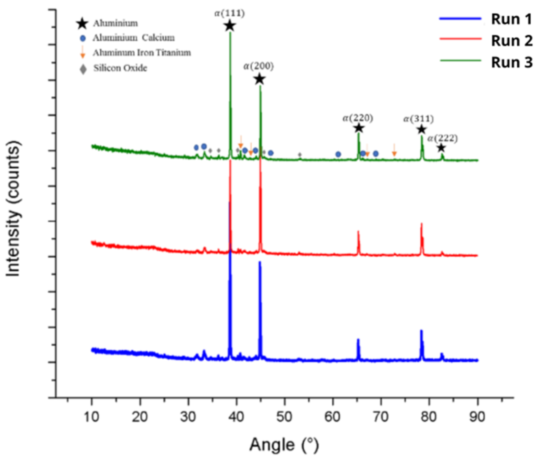

Fig. 11. X-ray diffraction patterns for Run 1 (as-received sample), Run 2 and Run 3.

4 Conclusion

Thermal stress relieving markedly shapes the mechanical and crystallographic response of closed-cell aluminium alloy foams. The 500 °C/60 min treatment with 450 °C stabilization (Run 2) produced the best performance—compressive strength 2.88 N mm^{-2}, plateau stress 2.35 N mm^{-2}, and energy absorption 116.79 J (≈95% above as-received)—via refined, uniformly distributed precipitates that relax lattice strain and reduce residual stresses; by contrast, 550 °C/120 min (Run 3) caused precipitate coarsening and strength loss. These results establish a multiscale link between stress-relief parameters, lattice-strain relaxation, and macroscopic energy-dissipation behavior, offering actionable guidance for designing crash-resistant, lightweight foam structures. The study is limited to two temperature–time windows under vacuum, uses XRD/EDX without TEM/EBSD, and performs compressive tests only in a quasi-static manner. Future work should broaden the thermal space (including cooling rate and atmosphere), apply TEM/EBSD to resolve precipitate–dislocation interactions, and assess cyclic and high-rate loading to build predictive process–structure–property models. Overall, we provide compact evidence that optimized low-temperature stress relief enhances mechanical reliability by tuning crystallographic distortion—adding new knowledge and a practical pathway for post-processing aluminium foam.

References

1. O. V. Byakova, S. Gnyloskurenko, A. O. Vlasov, Y. Yevych, N. Semenov, and D. Kytranov, The role of cell collapse mechanism in mechanical performance of aluminium foam fabricated by melt processing. Key Eng Mater. **2024**, (2024). https://doi.org/10.4028/p-03cmzt
2. A. Gopinathan, J. Jerz, J. Kováčik, and T. Dvořák, Investigation of the relationship between morphology and thermal conductivity of powder metallurgically prepared aluminium foams. Materials. **14**, 3623 (2021). https://doi.org/10.3390/ma14133623
3. G. Epasto, F. Distefano, H. Mozafari, E. Linul, and V. Crupi, Nondestructive evaluation of aluminium foam panels subjected to impact loading. Applied Sciences. **11**, 1148 (2021). https://doi.org/10.3390/app11031148
4. M. S. Raza, S. Datta, and P. Saha, Thermal and morphological analysis of the interaction effect of different assist gases with gas-filled closed-cell aluminium foam during laser cutting process. Proc Inst Mech Eng B J Eng Manuf. **2020**, (2020). https://doi.org/10.1177/0954405420917252
5. T. Fiedler and N. Movahedi, Compact aluminium foam heat exchangers. Metals (Basel). **13**, 1440 (2023). https://doi.org/10.3390/met13081440
6. M. Brůna, I. Vasková, and M. Galčík, Numerical simulation and experimental validation of melt flow

in the naturally pressurized gating system. Processes. **9**, 1931 (2021). https://doi.org/10.3390/pr9111931

7. D. Izzatus Tsamroh, D. Puspitasari, P. Puspitasari, and M. Mustapha, Microstructure and hardness study of Al6061 resulting from artificial aging. Vokasi Unesa Bulletin of Engineering, Technology and Applied Science. **2**, 48–56 (2025). https://doi.org/10.26740/vubeta.v2i1.34984
8. I. Nová, K. Fraňa, P. Solfronk, D. Koreček, and J. Sobotka, Properties of aluminium cellular materials produced by powder metallurgy using the foaming agent TiH_2. Manufacturing Technology. **22**, (2022). https://doi.org/10.21062/mft.2022.051
9. H. Basri, J. Jalaluddin, R. Tarakka, M. Syahid, and M. A, Ilahi Rahmadhani. Study of modified absorber plate with aluminium foam of solar water heating system. Applied Mechanics and Materials. **2023**, (2023). https://doi.org/10.4028/p-u5qx47
10. M. Madgule, P. V. L. Sagar, S. Palanisamy, K. V. V. R. Rao, M. V, Reddy, and R. R. Kumar. Influence of foaming agents on mechanical and microstructure characterization of AA6061 metal foams. Proceedings of the Institution of Mechanical Engineers Part E Journal of Process Mechanical Engineering. **2022**, (2022). https://doi.org/10.1177/09544089221097534
11. Y. Zhao, C. Yunfei, L. Li, J. Zhang, and C. Xiukang, Experimental and finite element simulation study of the mechanical behaviors of aluminum foam-filled single/double tubes. Mater Res Express. **2023**, (2023). https://doi.org/10.1088/2053-1591/acc2a4
12. L. Cui, Y. Li, W. Zhang, J. Liu, T. Liu, and Z. Fan, Compression fatigue properties of closed-cell aluminum alloy foams fabricated by two-step foaming method. Adv Eng Mater. **2025**, (2025). https://doi.org/10.1002/adem.202402769
13. J. Wang, Y. Wang, X. He, T. Wang, and C. Li, Axial impact performances of composite aluminum foam tubes. Adv Eng Mater. **2024**, (2024). https://doi.org/10.1002/adem.202400897
14. Y. Hangai, T. Takagi, Y. Goto, and K. Amagai, Fabrication of two-layer aluminum foam consisting of dissimilar aluminum alloys using optical heating. Materials. **17**, 894 (2024). https://doi.org/10.3390/ma17040894
15. W. D. Callister Jr and D. G. Rethwisch, Materials science and engineering: an introduction. John Wiley & Sons. **2020**, (2020).
16. H. Zhang, M. Lei, Z. Lin, W. Gong, J. Shen, and Y. Zhang, The compressive properties and deformation mechanism of closed-cell aluminum foam with high porosity after high-temperature treatment. Sustainability. **14**, 9850 (2022). https://doi.org/10.3390/su14169850
17. F. Rahimidehgolan and W. Altenhof, Compressive behavior and deformation mechanisms of rigid polymeric foams: a review. Composites Part B. **110513**, (2023). https://doi.org/10.1016/j.compositesb.2023.110513
18. Y. Xiao, J. Yin, X. Zhang, X. An, Y. Xiong, and Y. Sun, Mechanical performance and cushioning energy absorption characteristics of rigid polyurethane foam at low and high strain rates. Polym Test. **109**, (2022). https://doi.org/10.1016/j.polymertesting.2022.107531
19. M. A. A. Hasan, K. A. Jasim, and H. A. J. Miran, Synthesis and comparative analysis of crystallite size and lattice strain of $Pb_2Ba_{1.7}Sr_{0.3}Ca_2Cu_3O_{10+\delta}$ superconductor. Korean J Mater Res. **32**, 66–71 (2022). https://doi.org/10.3740/MRSK.2022.32.2.66
20. J. Rakhmonov, K. Liu, P. Rometsch, N. Parson, and X.-G. Chen, Improving the mechanical response of Al–Mg–Si 6082 structural alloys during high-temperature exposure through dispersoid strengthening. Materials. **13**, 5295 (2020). https://doi.org/10.3390/ma13225295
21. Z. Xu, H. Ma, N. Zhao, and Z. Hu, Investigation on compressive formability and microstructure evolution of 6082-T6 aluminum alloy. Metals (Basel). **10**, 469 (2020). https://doi.org/10.3390/met10040469
22. M. S. Kim, D.-Y. Kim, Y. Do Kim, H. Choi, and S. H. Kim, Archives of Metallurgy and Materials. **2021**, (2021). https://doi.org/10.24425/amm.2021.136380
23. B. Parveez, N. A. Jamal, H. Anuar, Y. Ahmad, A. Aabid, and M. Baig, Microstructure and mechanical properties of metal foams fabricated via melt foaming and powder metallurgy technique: a review. Materials. **15**, 5302 (2022). https://doi.org/10.3390/ma15155302
24. N. K. Singh and S. Balaguru, Development and characterization of aluminium AA7075 hybrid composite foams (AHCFs) using SiC and TiB_2 reinforcement. **2022**, (2022). https://doi.org/10.21203/rs.3.rs-1718478/v1
25. F. Garai. Modern applications of aluminium foams, Int J Eng Manag Sci. **5**, 14–21 (2020). https://doi.org/10.21791/ijems.2020.2.3
26. K. Grilec, I. Bunjan, and S. Jakovljević, The influence of applied force on aluminium foams energy absorption. Tehnicki Vjesnik - Technical Gazette. **2021**, (2021). https://doi.org/10.17559/tv-20200109101038
27. A. K. Srivastava, N. K. Maurya, M. Maurya, S. P. Dwivedi, and A. Saxena, Effect of multiple passes on microstructural and mechanical properties of surface composite Al 2024/SiC produced by friction stir processing. Annales De Chimie Science Des Matériaux. **44**, (2020). https://doi.org/10.18280/acsm.440608
28. A. J. Ansari and M. Anas, Review and analysis of the effect of variables on aluminium based surface composite fabricated through friction stir processing method. Int J Adv Technol Eng Explor.

9, (2022). https://doi.org/10.19101/ijatee.2021.875903

29. N. M. Siddesh Kumar, S. P. Chethan, T. G. Nikhil, and Dhruthi, A review on friction stir processing over other surface modification processing techniques of magnesium alloys. Funct Compos Struct. **4**, (2022). https://doi.org/10.1088/2631-6331/ac49f3